Articles

Secondary Structure, Orientation, Oligomerization, and Lipid Interactions of the Transmembrane Domain of Influenza Hemagglutinin†

Suren A. Tatulian‡ and Lukas K. Tamm*

Department of Molecular Physiology and Biological Physics and Center for Structural Biology, University of Virginia Health Sciences Center, Charlottesville, Virginia 22908-0736

Received July 9, 1999; Revised Manuscript Received October 18, 1999

ABSTRACT: Influenza virus hemagglutinin (HA), the viral envelope glycoprotein that mediates fusion between the viral and cellular membranes, is a homotrimer of three subunits, each containing two disulfide-linked polypeptide chains, HA_1 and HA_2. Each HA_2 chain spans the viral membrane with a single putative transmembrane α-helix near its C-terminus. Fusion experiments with recombinant HAs suggest that this sequence is required for a late step of membrane fusion, as a glycosylphosphatidylinositol-anchored analogue of HA only mediates "hemifusion" of membranes, i.e., the merging of the proximal, but not distal, leaflets of the two juxtaposed lipid bilayers [Kemble et al. (1994) *Cell 76*, 383−391]. To find a structural explanation for the function of the transmembrane domain of HA_2 in membrane fusion, we have studied the secondary structure, orientation, oligomerization, and lipid interactions of a synthetic peptide representing the transmembrane segment of X:31 HA (TMX31) by circular dichroism and attenuated total reflection Fourier transform infrared spectroscopy and by gel electrophoresis. The peptide was predominantly α-helical in detergent micelles and in phospholipid bilayers. The helicity was increased in lipid bilayers composed of acidic lipids compared to pure phosphatidylcholine bilayers. In planar lipid bilayers, the helices were oriented close to the membrane normal. TMX31 aggregated into small heat-resistant oligomers composed of two to five subunits in SDS micelles. Amide hydrogen exchange experiments indicated that a large fraction of the helical residues were accessible to water, suggesting the possibility that TMX31 forms pores in lipid bilayers. Finally, the peptide increased the acyl chain order in lipid bilayers, which may be related to the preferential association of HA with lipid "rafts" in the cell surface and which may be an important prerequisite for complete membrane fusion.

The homotrimeric surface glycoprotein of the influenza virus envelope, hemagglutinin (HA),[1] plays a major role in infection by mediating virus entry into host cells and fusion between viral and cellular target membranes (see refs *1* and *2* for review). HA consists of two polypeptide chains, HA_1 and HA_2, which are primarily responsible for receptor binding and membrane fusion, respectively. After endocytosis of the virion, the mildly acidic milieu of the endosome induces a major conformational change in HA (*3*, *4*), which eventually results in membrane fusion and the release of the nucleocapsid into the cytoplasm. The N-terminus of the HA_2 chain is formed by a moderately hydrophobic peptide, the so-called "fusion peptide". At neutral pH, the fusion peptide is buried in the core of the native protein trimer (*5*), but it becomes exposed and inserted into the target membrane under fusion conditions at low pH (*6*, *7*). The HA_2 chain also contains a single transmembrane (TM) domain near its C-terminus that anchors HA in the viral envelope. As shown by photoaffinity labeling, the transmembrane and the fusion peptides are the only segments of HA that interact directly with the lipid bilayers of the host and target membranes (*8*). Therefore, these segments must be intimately involved in the process of membrane fusion. Considerable efforts have been directed toward elucidating the structure and interactions of the fusion peptide in lipid bilayers (see, e.g., refs *9*−*13*). However, much less work has focused so far on studying structure−function relationships of the TM domain of influenza HA.

There is substantial evidence that the TM domain is important for several aspects of HA function, beyond

† Supported by NIH Grant AI30557.

* Corresponding author. Phone: (804) 982-3578. FAX: (804) 982-1616. E-mail: lkt2e@virginia.edu.

‡ Present address: Department of Molecular Biosciences, 7042 Haworth Hall, University of Kansas, Lawrence, KS 66045-2106.

[1] Abbreviations: ATR, attenuated total reflection; CD, circular dichroism; CMC, critical micelle concentration; DMF, dimethylformamide; DMPC, 1,2-dimyristoyl-*sn*-glycero-3-phosphocholine; DMPG, 1,2-dimyristoyl-*sn*-glycero-3-phosphoglycerol; EDTA, ethylenediaminetetraacetic acid; FTIR, Fourier transform infrared; GPI, glycosyl-*sn*-glycero-3-phosphoinositol; HA, hemagglutinin; HBTU, *O*-benzothiazole-*N*,*N*,*N*′,*N*′-tetramethyluronium hexafluorophosphate; HFIP, hexafluoro-2-propanol; lysoPC, 1-dodecyl-2-hydroxyphosphatidylcholine; MALDITOF, matrix-assisted laser desorption ionization time-of-flight; PAGE, polyacrylamide gel electrophoresis; SDS, sodium dodecyl sulfate; TFA, trifluoroacetic acid; TM, transmembrane; TMX31, 30-residue peptide of strain X:31 influenza HA.

10.1021/bi991594p CCC: $19.00
Published on Web 12/20/1999

providing a simple membrane anchor for HA_2. For example, when the TM domain of HA was substituted with a glycosylphosphatidylinositol (GPI) anchor, the resulting molecules were only able to mediate hemifusion, i.e., the merging of the proximal, but not the distal, leaflets of the two juxtaposed lipid bilayers (*14*−*16*). Obviously, fusion was blocked at an intermediate step under these conditions. Since the conformational change and the insertion of the fusion peptide into target membranes were still promoted by the GPI-anchored HA, the hemifusion intermediate is a relatively late intermediate in the fusion reaction. Consequently, the TM domain is thought to promote progression to the full fusion pore by breaking the hemifusion diaphragm by a mechanism that is still poorly understood. This role can be strictly attributed to the TM domain because recombinant HAs, in which the intraviral tail, i.e., the ~12 most C-terminal residues of HA_2, had been deleted, still promoted full membrane fusion (*17*). This C-terminal tail contains three conserved palmitoylated cysteines that are not required for fusion either, as shown by fusion experiments with HAs, in which these cysteines were either individually or collectively ablated by mutagenesis (*18*). Finally, recent studies indicate that not even the specific sequence of the influenza HA TM domain is required for the completion of membrane fusion; when the TM domain of influenza HA_2 was replaced by the TM domain of the analogous F glycoprotein of Sendai virus, the fusion activity of the chimeric protein was not altered (*19*).

The TM domain of HA has another important function: It plays a critical role in the folding and delivery of this protein to detergent-resistant lipid "rafts" in the apical plasma membrane (*20*). In contrast to its involvement in a late step of membrane fusion, this latter function critically depends on the specific sequence of the TM domain. Site-directed mutations within this domain impair the ability of HA to segregate into lipid rafts in the cell surface (*21*). Residues residing in the outer leaflet of the membrane seem especially important for targeting HA to lipid rafts in the apical membrane. For example, in Japan HA Ile511(186), Val 512-(187), Thr517(192), Val518(193), Gly520(195), and Ser521-(196)[2] are crucial for the proper assembly of HA in lipid rafts, while other residues in that region are less important (*22*). Changing Ile-514(189) and Tyr-515(190) to alanines inhibits the delivery of HA to the cell surface and therefore, presumably, the correct assembly (folding) of the TM domains in the lipid bilayer of the endoplasmic reticulum (*22*).

Despite the importance of the TM domain of influenza HA in membrane fusion and assembly in the cell surface, no studies have been undertaken thus far to assess the structure of this peptide in lipid bilayers and the mode of its interaction with membrane lipids. To probe the structure and lipid interactions of the TM domain of HA, we synthesized a 30-residue peptide (TMX31) which was modeled after the sequence of the TM domain of the strain X:31 influenza HA and spectroscopically characterized this peptide in various environments. TMX31 was highly α-helical in membrane-mimetics and lipid bilayers. The peptide exhibited a strong potential for self-association and was oriented close to the membrane normal, possibly forming a water-accessible oligomer in the lipid bilayer. Finally, TMX31 increased the acyl chain order of the surrounding lipids. Ordering of the acyl chains is likely coupled to dehydration at the membrane surface, which could be one aspect of the mechanism by which the TM domain of HA facilitates membrane fusion.

[2] Numbers in parentheses use the X:31 aligned HA_2 numbering system that was employed in Figure 1.

MATERIALS AND METHODS

Peptide Synthesis. TMX31 was synthesized by Dr. V. Kalashnikov by the solid-phase method using the Fmoc/t-Bu strategy on a Rainin Symphony peptide synthesizer. The Rink amide poly(ethylene glycol)/polystyrene resin with 0.15 mmol/g substitution was utilized as a solid support. The following amino acid side chain protections were used: t-Bu (Asp and Ser), t-Boc (Lys and Trp), Pbf (Arg), and Trt (Cys and Gln). Normally, amino acids (4 equiv) were coupled with peptide-resin by addition of 4 equiv of HBTU (activator) and 16 equiv of diisopropylethylamine (base). In the case of incomplete reaction, the coupling was repeated with 5 equiv of a symmetric anhydride of the requisite amino acid. Unreacted α-amino groups remaining after each coupling reaction were capped by 10 min treatment with 10% acetic anhydride in DMF. Fmoc deprotection was effected using 25% piperidine in DMF. The peptide was cleaved from the solid support, and all side-chain protecting groups were removed simultaneously by treatment of the peptide-resin with a mixture of TFA/H_2O/*m*-cresol/thioanisole/ethanedithiol (82.5:5:5:5:2.5, v/v) at room temperature for 3 h. After filtration, the crude product was precipitated with cold diethyl ether. The peptide was dissolved in a minimal volume of HFIP and purified with an H_2O (0.05% TFA) vs acetonitrile gradient on a ZORBAX StableBond C-3 reverse phase HPLC column at 65 °C. The identity of the peptide was checked by MALDITOF mass spectroscopy and by amino acid composition. The peptide was >90% pure as determined by HPLC. Concentrations of peptide stock solutions were determined by quantitative amino acid analysis. For the preparation of ^{13}C-labeled peptides, Fmoc-protected (1-^{13}C)-labeled amino acids were either purchased from Cambridge Isotope Laboratories (Andover, MA) or made from the (1-^{13}C)-labeled L-amino acids following a published procedure (*23*). The synthesized Fmoc-^{13}C-amino acids were crystalline and were >95% pure as judged by analytical HPLC.

Sodium Dodecyl Sulfate−*Polyacrylamide Gel Electrophoresis.* SDS−PAGE was performed using 12−20% linear gradient gels following the procedures of Porzio and Pearson (*24*) and Jones et al. (*25*) with slight modifications. The gel was prepared using 12% and 20% acrylamide solutions containing *N*,*N*′-methylenebisacrylamide at an acrylamide:bisacrylamide molar ratio of 30:1 in an aqueous buffer of 0.1% SDS, 5% glycerol, 0.06 mM EDTA, 0.3 M glycine, and 0.1 M Tris (pH 8.8). Approximately 0.12% ammonium persulfate and 0.15% tetramethylenediamine were added to the solutions in the two compartments of the gradient maker immediately before casting the gel. The 0.75 mm thick slab gels were overlaid with H_2O-saturated 1-butanol and allowed to polymerize for 2 h. The stacking gel was prepared using a 4% acrylamide solution in the same buffer and same acrylamide:bisacrylamide ratio. Peptide samples for electrophoresis were prepared by mixing the peptide in HFIP with lysoPC in ethanol, removing the solvent under vacuum, adding 20 μL of aqueous buffer (0.1 M NaCl, 10 mM Hepes,

pH 7.2), and vortexing. The peptide and lysolipid concentrations were ~0.5 and 3 mM, respectively. This was followed by addition of 20 μL of "treatment" buffer (0.125 M Tris, 4% SDS, 20% glycerol, 10% 2-mercaptoethanol, pH 6.8) and vortexing. The samples were divided into two equal parts, one of which was immersed in boiling water for 3 min while the other was kept at room temperature. Electrophoresis was conducted at 20 mA constant current for 1.75 h using a tank buffer containing 25 mM Tris, 0.2 M glycine, and 0.1% SDS, pH 8.3. The gels were stained with 0.025% Coomassie Brilliant Blue R-250. The wet gels were used for the preparation of figures and for quantitation using Image Quant version 1.2.

Reconstitution of the Peptide into Lipid Vesicles and Supported Lipid Bilayers. The peptide was solubilized in lysoPC micelles by mixing appropriate amounts of TMX31 in HFIP and lysolipid in ethanol, removing the organic solvents by a flow of nitrogen and then by high vacuum for ~1 h, adding aqueous buffer to a final concentration of [lysoPC] = 3 mM, and vortexing. These samples were used for CD measurements in lysoPC and for reconstitution of TMX31 into lipid vesicles. Phospholipid vesicles were prepared by extrusion of a vortexed lipid dispersion through 100 nm pore size polycarbonate membranes (Nucleopore, Pleasanton, CA) using a Liposofast extruder (Avestin, Ottawa, Canada). Reconstitution of the peptide into the vesicles was performed by mixing 1 volume of solubilized peptide in lysoPC with 9 volumes of ~100 nm vesicles so that the final concentrations of lysoPC and phospholipid were 0.3 and 1 mM, respectively. The lysolipid concentrations were chosen to be above the CMC before and below the CMC (0.9 mM for dodecyl-lysoPC) after dilution into the phospholipid suspension, which ensured incorporation of the peptide into lipid bilayers. For the reconstitution of the peptide into supported bilayers, a phospholipid monolayer was first deposited onto a 50 × 20 × 1 mm^3 germanium internal reflection plate (Spectral Systems, Irvington, NY) using Langmuir−Blodgett equipment (Nima model 611, Coventry, England). The plate with the monolayer was assembled in a perfusable liquid ATR cell, and the vesicles with the reconstituted peptide were incubated in the cell at room temperature for ~1.5 h. This procedure allowed the vesicles to spread on the monolayer, yielding supported phospholipid bilayers containing reconstituted TMX31 (*26*, *27*).

Circular Dichroism and Fourier Transform Infrared Spectroscopy. CD measurements were carried out at 20 °C on a Jasco J-720 spectropolarimeter (Jasco, Easton, MD) using 0.5 mm path length cuvettes. All spectra were recorded at 30 μM peptide in 2.5 mM phosphate buffer, pH 7.4. Three scans were averaged, and reference spectra of the respective media were subtracted. ATR-FTIR experiments were performed at room temperature on a Nicolet 740 infrared spectrometer (Nicolet Analytical Instruments, Madison, WI) in D_2O buffer (150 mM NaCl, 10 mM Tris-HCl, pH* 7.0) as described (*28*). The spectra were recorded at 2 cm^{-1} nominal resolution, and 1000 scans were co-added. For amide hydrogen/deuterium (H/D) exchange experiments, the supported bilayers were prepared in an H_2O buffer (150 mM NaCl, 10 mM Tris-HCl, pH 7.4). After recording an initial spectrum, the cell was flushed with 10−12 volumes of D_2O buffer. The time point of the injection of the D_2O buffer was taken as the zero time of H/D exchange. Spectra were recorded in rapid succession in the first 2 h and at 32 min intervals at later times. Only 552 scans were co-added in these spectra, which turned out to be a good compromise between defining the "time point" of each spectrum and an acceptable signal-to-noise ratio.

Data Analysis. The fraction of residues in the α-helical conformation, f_H, was estimated from the measured mean residue ellipticity at 222 nm, θ_{222}, using the standard equation:

$$f_H = (\theta_{222} - \theta_C)/(\theta_H - \theta_C) \quad (1)$$

where θ_H and θ_C are the limiting values of θ_{222} for completely helical and completely random coil peptides, respectively. θ_H depends on the temperature, T, in centigrade and on the number of amino acid residues in the polypeptide chain, n, as determined by Luo and Baldwin (*29*):

$$\theta_H = (250T - 44000)(1 - 3/n) \quad (2)$$

The value of θ_C depends on temperature and on the solvent environment. In 50% trifluoroethanol and at 20 °C, θ_C = −3400 deg × cm^2 × dmol^{-1} (*30*). For our 30-residue peptide in hydrophobic environments (micelles or lipid bilayers) at 20 °C, we have used θ_H = −35 100 and θ_C = −3400 deg × cm^2 × dmol^{-1}.

ATR dichroic ratios, R^{ATR}, of the lipid or peptide absorbance bands in supported bilayers were measured in polarized ATR-FTIR experiments as $R^{ATR} = A_{\parallel}/A_{\perp}$, where $A_{\parallel}$ and $A_{\perp}$ are the peak absorbancies at parallel and perpendicular polarizations of the incident infrared light. Order parameters, S, describing lipid and peptide order in supported bilayers were determined from the measured R^{ATR} values using the formula:

$$S = \frac{2B}{f(3\cos^2\alpha - 1)(B - 3E_z^2)} \quad (3)$$

where $B \equiv E_x^2 - R^{ATR}E_y^2 + E_z^2$ (*27*). E_x, E_y, and E_z are the components of the evanescent electric field at the germanium/water interface, f is the fraction of transition dipoles in the molecule that belong to the ordered structure of the absorption band of interest, and α is the angle between the transition dipole moment and the ordered structure. We used two different models to calculate the order parameters, i.e., the thin film approximation, which takes into account the influence of the supported bilayer on the normal component of the electric field E_z, and the two-phase model, which disregards this effect. Given an incidence angle of 45° and the indices of refraction of the germanium plate, the lipid bilayer, and the aqueous buffer of 4.0, 1.43, and 1.33, respectively, $E_x^2 = 1.969$, $E_y^2 = 2.249$, and $E_z^2 = 1.892$ in the thin film model. E_z^2 changes to 2.528 in the two-phase model. The angle α between the transition dipole moment of the amide I vibration and an α-helix is 39°, and the values of $f = f_H$ are taken from the CD measurements according to eq 1. To calculate order parameters of the lipid acyl chains from the dichroic ratios of the symmetric and antisymmetric methylene stretching vibrations, f is set to 1 and α is set to 90° in eq 3. The angles of orientation of the molecular axis with respect to the membrane normal, θ, are averaged by

$$S = \frac{1}{2}(3\langle\cos^2\theta\rangle - 1) \quad (4)$$

The peptide-to-lipid molar ratio, *P/L*, in the supported bilayer was estimated by

$$\frac{P}{L} = \frac{A_{\perp P}\sigma_L\epsilon_L n_L}{A_{\perp L}\sigma_P\epsilon_P n_P} \quad (5)$$

where $\sigma_i = (S_i \sin^2 \alpha_i)/2 + (1 - S_i)/3$, ϵ_i is the extinction coefficient per active chemical group of the respective absorption band, and n_i is the number of peptide bonds or lipid CH_2 groups for $i = P$ and $i = L$, respectively (*27*).

In amide H/D exchange experiments, the fraction of nonexchanged residues was determined as

$$\left(\frac{H}{H+D}\right)_t = \frac{(A_{\text{amideII}})_t}{(A_{\text{amideII}})_0} \quad (6)$$

and its time dependence was expressed as (*31*)

$$\left(\frac{H}{H+D}\right)_t = a_0 + a_1 e^{-k_1 t} + a_2 e^{-k_2 t} \quad (7)$$

Here, t is a time point in the course of H/D exchange and time 0 corresponds to a time point before replacement of H_2O by D_2O. The parameters a_0, a_1, and a_2 are the fractions of H/D exchange-resistant, slowly exchanging, and fast exchanging residues, respectively, and k_1 and k_2 are the rate constants of slow and fast exchange, respectively.

RESULTS

Sequence Conservation in HA Transmembrane Domains of Different Influenza Strains. Strains of avian and mammalian influenza A viruses have been divided into 14 subtypes (serotypes) based on distinct antigenic determinants of their hemagglutinins (*32*, *33*). In Figure 1, we compare the sequences of the putative transmembrane domains of representative HAs of all 14 subtypes. Although the sequences are characterized by high average hydrophobicities between residues 185 and 211 (X:31 HA_2 chain numbering), they all contain several polar residues (mostly serines, but also some cysteines and threonines) dispersed throughout the hydrophobic core. Some of these residues, especially those in the N-terminal half of the TM domain, are highly conserved. A number of hydrophobic residues are also conserved to a high degree among different subtypes. These include Ile186, Leu187, Ile189, Leu197, and Trp208, which have 93, 100, 86, 79, and 71% identity, respectively. A glycine in position 204 and cysteine 210, which is the first of three palmitoylated residues that flank the C-terminus of the TM domain, are also highly conserved. Despite these remarkable inter-subtype sequence similarities, the sequences presented in Figure 1 can apparently be divided into two classes, one including subtypes H1, H2, H5, H6, H8, H9, H11, H12, and H13 and the other including subtypes H3, H4, H7, H10, and H14. These two classes have been designated the H1 and H3 groups, respectively (*32*).[3] The TM sequences of different H3 strains are also compared in Figure 1. They exhibit a very high degree of identity. In this work, we studied a synthetic 30-residue peptide corresponding to the putative transmembrane segment of a H3 subtype HA, namely, that of A/Hong Kong/1968 (or X:31) hemagglutinin. The sequence of this peptide (TMX31), which includes a few charged residues at either end of the hydrophobic core region, is presented in the middle of Figure 1.

Secondary Structure of TMX31 in Different Environments As Determined by CD Spectroscopy. Far-UV CD spectra of the TMX31 peptide dissolved in HFIP, solubilized in lysoPC micelles, and reconstituted in dimyristoylphosphatidylcholine (DMPC) and dimyristoylphosphatidylglycerol (DMPG) lipid bilayers are presented in Figure 2. All spectra exhibit two minima at ~210 and ~224 nm, indicating a predominantly α-helical secondary structure of the peptide in all four environments. The mean residue molar ellipticities at 222 nm, $[\theta]_{222}$, in HFIP, lysoPC, DMPC, and DMPG are −18 880, −21 490, −23 050, and −33 650 deg × cm^2 × $dmol^{-1}$, respectively. Using eq 1, we find that the α-helical contents of TMX31 are 49, 57, 62, and 95% in the four respective environments. Interestingly, the ratio $[\theta]_{222}/[\theta]_{210}$ of TMX31 is significantly larger in HFIP and in lipid bilayers (1.1−1.2) than in lysoPC (0.93). Also, the parallel $\pi\pi^*$ transition at ~210 nm is slightly red shifted in the organic solvent and lipid bilayers. These features have been attributed to the formation of helical coiled coils (*34*, *35*), although alternative causes, e.g., different solvent interactions, may also explain the observed effects. The spectra of Figure 2 indicate a significant increase of the α-helical content of TMX31 in negatively charged bilayers of DMPG compared to bilayers composed of the zwitterionic lipid DMPC. To further investigate the effect of lipid charge on the helicity of TMX31, we measured CD spectra in mixed lipid bilayers of various DMPC/DMPG compositions. We found helical contents of 64%, 69%, 79%, 88%, and 95% for TMX31 in bilayers containing 10, 20, 40, 60, and 100 mol % DMPG, respectively (data not shown).

Orientation and Secondary Structure of TMX31 in Lipid Bilayers As Determined by Polarized ATR-FTIR Spectroscopy. Polarized ATR-FTIR absorbance spectra of supported phospholipid bilayers with and without reconstituted TMX31 in the region of the lipid carbonyl stretching and peptide amide I′ vibrations are shown in Figure 3. In these experiments, the first (substrate-exposed) monolayer was pure DMPC, and the second (bulk aqueous phase-exposed) monolayer was DMPC/DMPG (4:1). TMX31 incorporated into supported bilayers gives rise to a relatively narrow amide I′ band centered at ~1657 cm^{-1} (Figure 3C). This amide I′ band position indicates that the peptide is in a predominantly α-helical conformation (*27*, *36*). To search for possible further components, second-derivative spectra were calculated as presented in Figure 4 for peptides reconstituted at different peptide:lipid ratios into the bilayers. These spectra extend into the region of the lipid ester carbonyl band at 1730−1740 cm^{-1} (see below). The second derivatives of the amide I′ bands reveal no significant other components besides the major α-helical component at ~1657 cm^{-1}. However, the band shown in Figure 3C is quite asymmetric with significant additional intensity at the lower frequency edge. When we attempted to fit this band with Gaussian components, ~70% of the total band area was found in the major

[3] The H14 subtype was not included in the original classification because it was only identified later (*33*).

Strain	Subtype	Amino acid sequence
A/PUERTO RICO/8/34	H1	Q--**IL**A**I**Y**S**T**VASSL**V**L**LVSLGAISF**WM**C**SN**
A/JAPAN/305/57	H2	Q--**IL**A**I**YAT**VA**G**SL**S**LA**IMMA**G**ISF**WM**C**SN**
A/TURKEY/ONTARIO/7732/66	H5	Q--**IL**S**I**Y**S**T**VASSL**A**LA**IMVA**G**LSF**WM**C**SN**
A/SHEARWATER/AUSTRALIA/72	H6	Q--**IL**A**I**Y**S**T**V**S**SSL**V**L**VGLIIAVGL**WM**C**SN**
A/TURKEY/ONTARIO/6118/68	H8	**K**--**IL**S**I**Y**S**T**VA**A**SL**C**LA**ILIA**G**GLILGM**Q**N**
A/TURKEY/WISCONSIN/1/66	H9	**K**--**IL**T**I**Y**S**T**VASSL**V**LA**MGFAAFLF**WA**M**SN**
A/DUCK/ENGLAND/1/56	H11	**K**--**IL**S**I**Y**S**C**IASSL**V**LA**ALIM**G**FMF**WA**C**SN**
A/DUCK/ALBERTA/60/76	H12	**K**--**IL**S**I**Y**SS**V**ASSL**V**L**LLMII**G**GFIFG**C**Q**N**
A/GULL/MARYLAND/704/77	H13	**K**--**AL**S**I**Y**S**C**IASSV**V**L**VGLILSFIM**WA**C**S**S**
A/HONG KONG/1968 (X:31)	H3	(183)**K**DW**IL**W**IS**FA***I**S**C**F**L**L*CVVL*L*-*G**F**I*MW**A**C**Q**R(212)
		c-label *i-label*
A/MEMPHIS/1/71	H3	**K**DW**IL**W**IS**FA**ISCFL**LCVVLL-**G**FIM**WA**C**Q**R**
A/VICTORIA/3/75	H3	**K**DW**IL**W**IS**FA**ISCFL**LCVVLL-**G**FIM**WA**C**Q**K**
A/UDORN/307/72	H3	**K**DW**IL**W**IS**FA**ISCFL**LCVVLL-**G**FIMTA**C**Q**K**
A/EQUINE/ALGIERS/72	H3	**K**DW**IL**W**IS**FA**ISCFL**ICVVLL-**G**FIM**WA**C**Q**K**
A/DUCK/CZECHOSLOVAKIA/56	H4	**K**DI**IL**W**IS**FS**ISCFL**LV**A**LLL-AFIL**WA**C**Q**N**
A/FPV/ROSTOCK/34	H7	**K**DV**IL**WF**S**FGA**SCFL**L**LA**IAV-**G**LV-FI**C**VK
A/CHICKEN/GERMANY/N/49	H10	**K**DI**IL**WF**S**FGA**SCFV**L**LA**AVM-**G**LV-FF**C**LK
A/MALLARD/ASTRAKHAN/244/82	H14	**K**DI**IL**W**IS**FS**MSCFV**FV**A**LIL-**G**FVL**WA**C**Q**N**

FIGURE 1: Aligned amino acid sequences of the transmembrane segments of representatives of 14 subtypes and additional subtype H3 sequences of type A influenza hemagglutinins. The usual single-letter amino acid codes are used. Dashes are introduced to maximize sequence alignment. Letters in boldface refer to residues that are conserved in 50% or more of the sequences of all different subtypes, including a few conservative replacements as described in the text. Residues are numbered using the X:31 HA_2 numbering system. A synthetic peptide corresponding to the 30-residue sequence of strain A/Hong Kong/1968 (X:31) was used in this study. The N- and C-termini of the synthetic peptide were acetylated and amidated, respectively. Residues that were labeled with ^{13}C in the isotope-edited FTIR experiments are underlined.

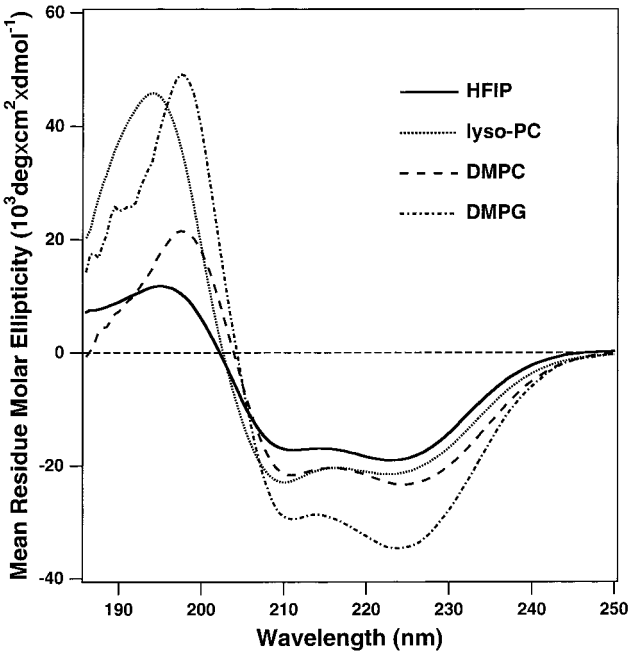

FIGURE 2: Circular dichroism spectra of TMX31 dissolved in hexafluoro-2-propanol (solid line), solubilized in 1-dodecyllysophosphatidylcholine (dotted line), and reconstituted in vesicles of DMPC (dashed line) or DMPG (dash−dotted line). All spectra were recorded at 20 °C.

component centered at 1657 cm^{-1} and at least two more ("virtual") components had to be introduced to fit the experimental band shape. Although β-structure is normally assigned to low-frequency amide I′ band components, FTIR spectra of several proteins that are known to have α-helical coiled coil structures exhibit components at 1639 and 1628 cm^{-1}, in addition to the major α-helical band at 1652 cm^{-1} (*37*, *38*). Residues in unordered conformations could also contribute to spectral intensity at ∼1645 cm^{-1} (*27*, *36*). Therefore, analysis of the amide I′ bands shows that TMX31 was 70−100% α-helical in planar lipid bilayers. This range is in approximate agreement with the CD results obtained with small unilamellar vesicles. The absence of a component that could be assigned to β-structure in the CD spectra, the high $[\theta]_{222}/[\theta]_{210}$ ratio observed in the CD spectra in lipid bilayers, and the asymmetric amide I′ band shape collectively may be taken as circumstantial evidence that TMX31 forms helical coiled coils in lipid bilayers. The dichroic ratio ($A_{\parallel}/A_{\perp}$) measured at 1657 cm^{-1} was ∼2.7 and, as shown in Table 1, decreased slightly as a function of the peptide:lipid ratio, although this trend is not clearly statistically significant. Order parameters and corresponding "average" orientations derived from the measured dichroic ratios are also listed in Table 1. The order parameters of the helical segment of the peptide are close to the limiting value of 1.0 (increasing from 0.83 with decreasing peptide concentrations). These order parameters were calculated assuming a helical fraction of 0.7 in 20 mol % DMPG, i.e., the value that was determined by CD spectroscopy. The high order parameters indicate that the helices of most TMX31 molecules in the sample are aligned perpendicular to the plane of the lipid bilayer. If all peptides were oriented at the same angle in a given sample, the measured order parameters would correspond to "average" tilt angles of the helix axis from the bilayer normal ranging from 0 to 26° as the concentration of the peptide increases in the lipid bilayer.

Oligomerization of TMX31 Assessed by SDS−PAGE. Since influenza hemagglutinins are noncovalent homotrimers and since at least three or four trimers are required for fusion (*39*, *40*), it is interesting to ask whether the TM domain itself has properties that would promote its aggregation into oligomers. The spectroscopic results described above provide circumstantial evidence that TMX31 formed coiled coils in lipid bilayers. To directly test whether TMX31 has the ability to self-associate in a membrane-mimetic environment, we conducted SDS−PAGE experiments using gradient gels. As shown in Figure 5, several bands were detected on these gels. The individual bands correspond to monomers, dimers,

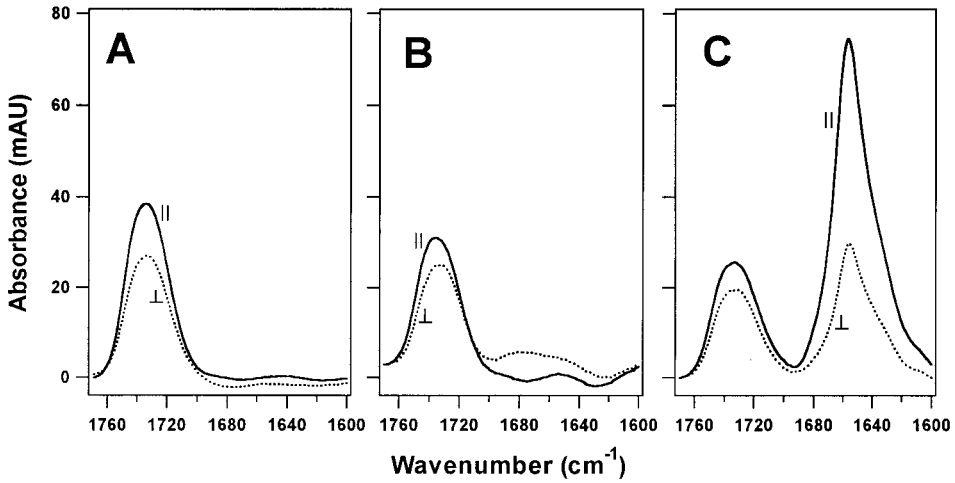

FIGURE 3: Polarized ATR-FTIR absorbance spectra of supported phospholipid bilayers without (panels A, B) and with (panel C) reconstituted TMX31 in the region of the lipid carbonyl stretching and peptide amide I′ vibrations. Solid and dotted lines correspond to parallel and perpendicular polarizations of the infrared light, respectively. Panel A was a pure DMPC bilayer that was prepared without using lysolipid. The bilayers of panels B and C were prepared using DMPC in the substrate-exposed monolayer and DMPC/DMPG (4:1) in the second monolayer. The vesicle solution that was used to assemble the second monolayer by vesicle fusion contained 0.3 mM lysoPC. However, most lysoPC was removed by repeated washes of the bilayer prior to the measurements (see Materials and Methods, for more detail).

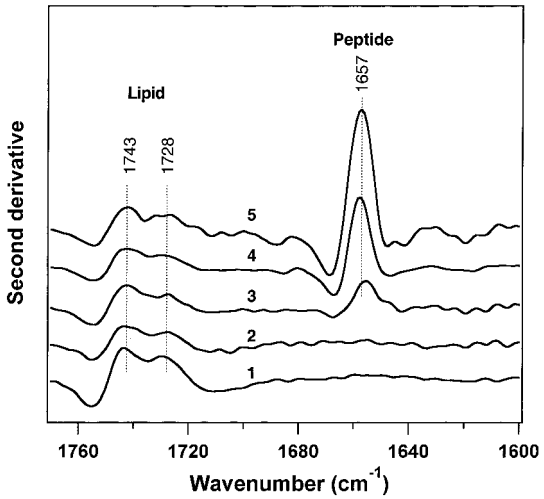

FIGURE 4: Second-derivative ATR-FTIR spectra of supported bilayers in the absence (curves 1 and 2) and presence of reconstituted TMX31 at peptide:lipid molar ratios of 0.005 (curve 3), 0.020 (curve 4), and 0.037 (curve 5). Spectrum 1 was recorded with a pure DMPC bilayer; all other spectra were obtained with DMPC/DMPC:DMPG (4:1) bilayers as described in the legend to Figure 3.

trimers, tetramers, and pentamers of TMX31. Higher order aggregates were not observed. Quantitative analysis of the gel (lane 3) shows that the relative fractions of these forms were approximately 17, 34, 23, 16, and 10%, respectively. Interestingly, these oligomers were extremely stable toward heat treatment. After boiling the sample for 3 min, the monomer-to-pentamer relative band intensities were 20, 30, 23, 19, and 8% (lane 2), i.e., not significantly different from those determined for the samples without boiling.

Amide Hydrogen Exchange of Membrane-Embedded TMX31. The oligomeric structure of TMX31 with several potential hydrogen bond donating residues within the TM region raises the interesting possibility that the complex may form a water-accessible pore in lipid bilayers. To evaluate water accessibility and to assess the dynamic properties of the TMX31 helices, we performed time-dependent amide H/D exchange experiments by ATR-FTIR spectroscopy. The spectra of Figure 6A demonstrate that after replacement of H_2O by D_2O, the amide I′ band shifts gradually toward lower frequencies and the amide II band at ∼1546 cm^{-1} substantially decreases in intensity. Amide I and amide II bands are known to typically shift toward lower frequencies by ∼10 and ∼90 cm^{-1}, respectively, upon H/D exchange (*27*). Therefore, we used the time-dependent reduction of the amide II band area to quantify the kinetics of H/D exchange of TMX31 using eqs 6 and 7. The results of this experiment are plotted in Figure 6B and show that the peptide contains three classes of residues with different hydrogen exchange kinetics: 42% of all residues exchange fast with a rate constant of 0.239 min^{-1}, 40% exchange slowly with a rate constant of 0.0116 min^{-1}, and 18% are resistant to amide hydrogen exchange over the time course of our experiments (12 h).

Local Structure and Dynamics of TMX31 by ^{13}C-Edited ATR-FTIR Spectroscopy. Site-directed labeling of the peptide bond carbons of specific amino acids with ^{13}C allows one to probe the local secondary structure and dynamics of peptides by FTIR spectroscopy. This approach is based on the fact that the amide I bands of individual secondary structures are shifted to lower frequencies by ∼35 cm^{-1} as a result of this isotope change (*41, 42*). To probe the structure of TMX31 in the central and the C-terminal (inner leaflet of the viral membrane) regions of the hydrophobic TM domain, we specifically labeled I_{193}, F_{196}, L_{197}, and L_{198} (c-labeled TMX31) and L_{203}, G_{204}, F_{205}, and I_{206} (i-labeled TMX31) of TMX31 with ^{13}C. Polarized ATR-FTIR spectra of these peptides in DMPC/DMPC:DMPG (4:1) bilayers are shown in Figure 7 2 min after H/D exchange (panels A and C, respectively) and 8.5 h after H/D exchange (panels B and D, respectively). Both peptides exhibit a distinct second component at ∼1628 cm^{-1} besides the primary component at ∼1657 cm^{-1}. This component grows in intensity as H/D exchange progresses. Because of this distinct feature, the amide I′ bands of these spectra could be easily decomposed into three components by unique fits (Figure 7). Two minutes after the H/D exchange was initiated, the primary (secondary) components occurred at 1659 (1631) and 1660 (1628) cm^{-1},

Table 1: Dichroic Ratios (R^{ATR}), Order Parameters (S), and "Average" Tilt Angles (θ) of the Reconstituted X:31 Hemagglutinin Transmembrane Peptide and Lipids in Supported Bilayers at Different Peptide/Lipid (P/L) Ratios, As Determined by ATR-FTIR Spectroscopy

	peptide			lipid	
P/L[a]	R^{ATR}	S^d	θ (deg)[d]	R^{ATR}	S^e
0[b]	N/A	N/A	N/A	1.38 ± 0.08	0.31 ± 0.08
0[c]	N/A	N/A	N/A	1.23 ± 0.03	0.48 ± 0.035
0.026 (0.005)	2.75 ± 0.17	1.02 ± 0.12	0−15	1.15 ± 0.03	0.58 ± 0.04
0.052 (0.020)	2.69 ± 0.11	0.98 ± 0.085	0−15	1.18 ± 0.04	0.54 ± 0.05
0.104 (0.037)	2.49 ± 0.14	0.83 ± 0.115	12−26	1.21 ± 0.02	0.51 ± 0.02

[a] The input and measured (in parentheses) peptide/lipid ratios are shown. P/L ratios in supported bilayers were determined by eq 5. [b] Pure DMPC bilayer. [c] DMPC/DMPC:DMPG (4:1) + 0. 3 mM lysoPC. [d] The values of S and θ were calculated by eqs 3 and 4 using the thin film approximation and $f_H = 0.7$ from the CD experiments. [e] The values of S were calculated by eq 3 using $f_H = 1$ and $\alpha = 90°$.

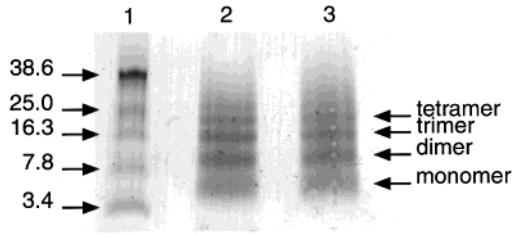

FIGURE 5: 12−20% gradient SDS−polyacrylamide gel showing the aggregation of TMX31 into oligomers. Lane 1: molecular mass standards. Lane 2: TMX31 loaded after boiling in SDS for 3 min. Lane 3: TMX31 loaded without prior boiling. The numbers at the left indicate the molecular masses of the standards in kDa, and the labels at the right indicate the different oligomerization states of the peptide.

for c- and i-labeled TMX31, respectively. A third component in the 1614−1618 cm^{-1} range was also present in these spectra. From a comparison of these spectra with those of Figure 3C, it is obvious that the components at ~1628 cm^{-1} arise from the ^{13}C-labeled residues in TMX31. The observed 28−32 cm^{-1} downshifts of these components relative to the primary components indicate that the labeled segments are also in a well-defined α-helical conformation, as will be discussed in more detail in the Discussion. The origin of the relatively small components at ~1616 cm^{-1} is not clear. These components are not immediately obvious in the unprocessed spectra and thus may be "artifacts" of trying to fit two superimposed asymmetric line shapes (i.e., those of the labeled and unlabeled residues, cf. Figure 3C) with symmetric Gaussian component bands. In the course of amide H/D exchange for 8.5 h, the peak frequencies of the primary components decreased to 1654 and 1657 cm^{-1}, i.e., by 5 and 3 cm^{-1}, for the c- and i-labeled peptides, respectively. By comparison, the frequencies of the secondary components, ascribed to the ^{13}C-labeled residues, decreased by only 2 cm^{-1} to 1629 cm^{-1} (c-labeled TMX31) or remained constant at 1628 cm^{-1} (i-labeled peptide) 8.5 h after H/D exchange. Since the ^{13}C-labeled residues of these peptides did not produce readily identifiable separate components in the amide II region (not shown), we were unable to separately evaluate the exchange kinetics of the labeled and unlabeled segments according to eq 7. Nevertheless, the comparatively small amide I band shifts upon H/D exchange indicate that in TMX31 the labeled residues are less susceptible to amide hydrogen exchange than the average unlabeled residues.

Effect of TMX31 on the Lipid Order. TMX31 exerts distinct effects on the host lipid bilayer structure both at the polar headgroup and at the hydrophobic acyl chain levels. The lipid carbonyl stretching band is composed of two components that vibrate at ~1743 and ~1728 cm^{-1} (Figure 4). These two vibrations are generated by relatively dehydrated and hydrated carbonyl groups, respectively (*43*). The second-derivative spectra presented in Figure 4 show that the component at 1728 cm^{-1} becomes less prominent upon incorporation of this peptide into the supported lipid bilayers. We tentatively interpret this result by a partial dehydration of the bilayer surface by the peptide. This interpretation is consistent with measurements performed at the level of the lipid hydrocarbon chains. Polarized ATR-FTIR spectra in the presence and absence of TMX31 show that incorporation of the peptide into lipid bilayers decreases the dichroic ratios of the CH_2 symmetric and antisymmetric stretching bands (Figure 8). According to eq 3, the observed decrease of the dichroic ratio corresponds to an increase of the acyl chain order parameter. The dichroic ratios and order parameters at different peptide:lipid molar ratios summarized in Table 1 show that the lipid order parameters increase from 0.3 in

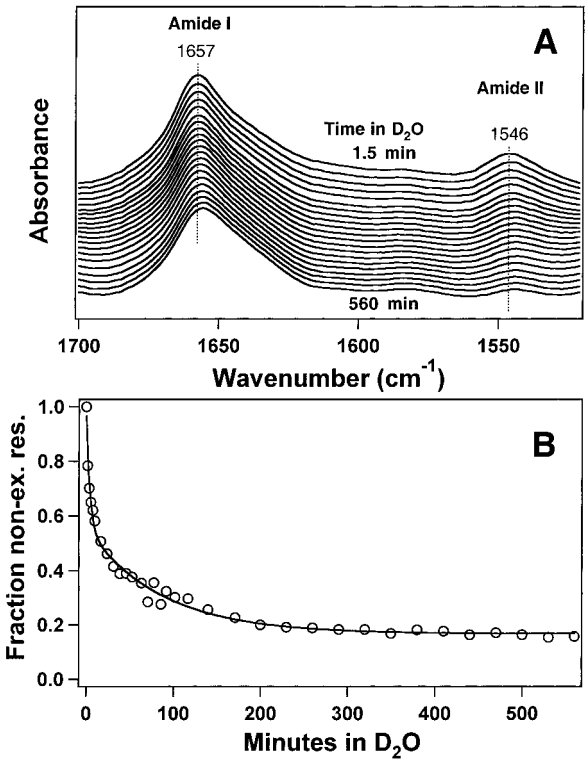

FIGURE 6: Amide hydrogen/deuterium exchange of TMX31 reconstituted in supported DMPC/DMPC:DMPG (4:1) bilayers. Panel A: Time-dependent changes of ATR-FTIR spectra in the amide I and amide II regions after replacing the H_2O with a D_2O buffer. Panel B: Time course of the fraction of nonexchanged amide hydrogens. The data points of panel B were calculated from the spectra of panel A using eq 6. The line represents the best fit of the data to eq 7.

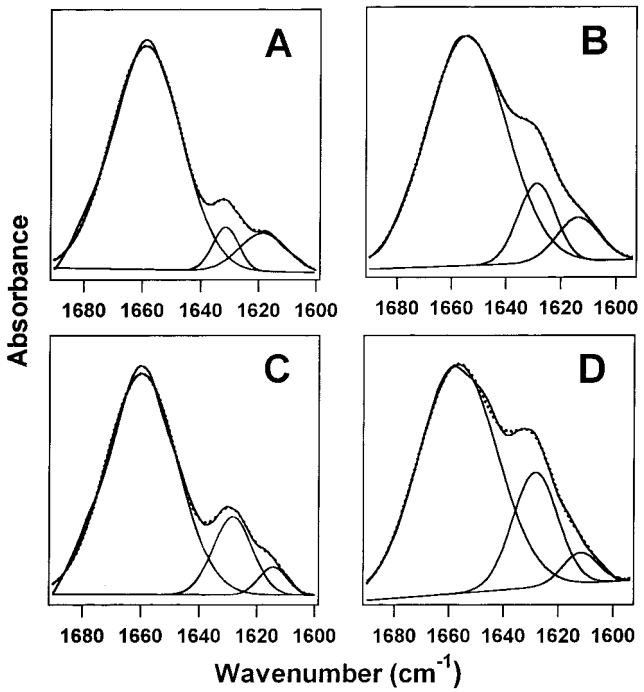

FIGURE 7: Polarized ATR-FTIR absorbance spectra in the amide I′ region of selectively ^{13}C-labeled TMX31's in supported DMPC/DMPC:DMPG (4:1) bilayers. Panels A and B: I_{193}, F_{196}, L_{197}, and L_{198} (c)-labeled TMX31. Panels C and D: L_{203}, G_{204}, F_{205}, and I_{206} (i)-labeled TMX31. The spectra of panels A and C were recorded 2 min after H/D exchange, and those of panels B and D 8.5 h after H/D exchange. The amide I′ bands are decomposed into Gaussian components. The calculated sums of the component bands are shown as dotted lines.

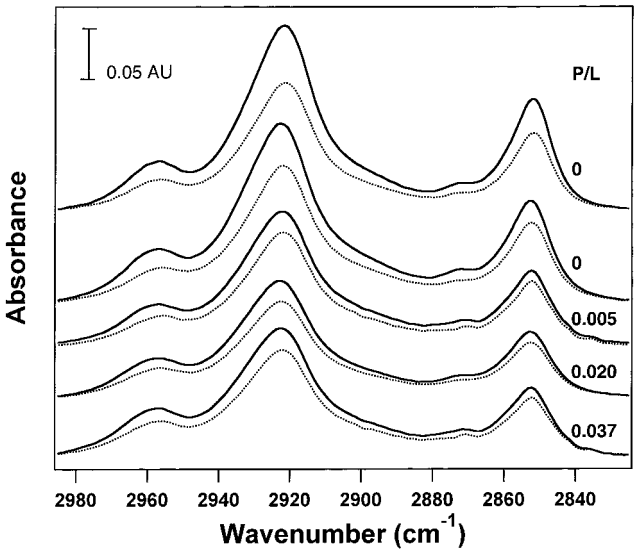

FIGURE 8: Polarized ATR-FTIR absorbance spectra of supported phospholipid bilayers without and with reconstituted TMX31 in the region of the lipid CH_2 stretching vibrations. Solid and dotted lines correspond to parallel and perpendicular polarizations of the infrared light, respectively. The upper pair of spectra corresponds to a pure DMPC supported bilayer. The other spectra correspond to DMPC/DMPC:DMPG (4:1) supported bilayers as described in the legend to Figure 3. The three lower pairs of spectra contain TMX31 at the indicated peptide:lipid molar ratios.

the absence to 0.5−0.6 in the presence of TMX31 in fluid DMPC/DMPG bilayers.

DISCUSSION

The goal of this work was to determine the general architecture of the transmembrane domain of influenza HA in lipid bilayers. This was accomplished by a combined spectroscopic and biochemical approach. We found that synthetic peptides that were modeled after the transmembrane sequence of strain X:31 HA indeed formed transbilayer helices as predicted. In addition, these helices had a strong tendency to self-associate into heat- and SDS-resistant oligomers, varying from dimers to pentamers, which possibly formed coiled coils in lipid bilayers. Isotope-edited FTIR spectra further helped to identify α-helical segments within the TM domains. It is interesting to consider these results vis-à-vis the degree of sequence conservation within the TM domains of different strains of influenza viruses. Comparison of the TM sequences of 14 strains from 14 different subtypes of influenza HAs shows that 3 regions are highly conserved (Figure 1). An N-terminal helical turn is almost invariably ILxIo in the H1 group or ILoIx in the H3 group of HAs (x = S in most cases, T or A in rare cases; o = large aromatic residue); a central conserved segment is hASSL in the H1 group and hSCFL in the H3 group (h = branched aliphatic residue, Leu197 is replaced by Val in a few strains); and Gly204, Trp208, and Cys210 are prevalent at the C-terminal end of the TM domain. Ile189 of the first conserved hydrophobic helical turn has been shown to be important for folding of HA in the membrane (*22*). In isotope-edited FTIR experiments, we found that the central conserved segment (marked "c-label" in Figure 1) and the C-terminal segment around Gly204 in the inner leaflet of the viral lipid bilayer (marked "i-label" in Figure 1) exhibited frequency-shifted amide I′ bands, which indicated unperturbed α-helices in these regions (see below). Therefore, the conserved SC-rich central and the hydrophobic inner leaflet segments assume normal α-helical secondary structures with similar FTIR characteristics in lipid model membranes.

All residues of the first two conserved regions, i.e., the ILxIo (ILoIx) and the hASSL (hSCFL) segments, seem important for targeting HA to lipid "rafts" (*20*−*22*). Lipid rafts are small domains in the plasma membrane that are enriched in sphingomyelin and cholesterol. The lipids in these domains have been shown to be more ordered than those in other regions of the plasma membrane (*44*, *45*). Our finding (Figure 8 and Table 1) that the synthetic TM peptide TMX31 increases the order of the acyl chains of the lipid bilayer in our model system may be related to the targeting of HA to more ordered domains in cell membranes. The mutual interactions between the TM peptide (oligomer) and the surrounding lipids seem to be reciprocal: Ordered lipids attract the TM domains, and the TM domains in turn order the lipids surrounding them. Relatively little is known about the effect of other TM helices on lipid order. For example, polyleucine helices seem to have little effect on lipid order in fluid bilayers as measured by ^{2}H NMR, even if there is considerable mismatch between the hydrophobic length of the helix and the hydrophobic thickness of the bilayer (*46*).[4] The effect of the TM domain of phospholamban on the order

[4] However, a short (16 hydrophobic residues) polyleucine-containing peptide had a disordering effect on a "thick" cholesterol-containing lipid bilayer (*46*). There are no reasons to assume that there is a large hydrophobic mismatch between TMX31 and the DMPC bilayers used in this study.

of the surrounding DMPC bilayer was measured, as here, by polarized ATR-FTIR spectroscopy and found to be smaller than observed here for TMX31 (*47*). Therefore, the ability of TMX31 to order lipids appears not to be a universal property of TM peptides, but may be specific to this (and perhaps other, yet to be discovered) sequence(s). It will be interesting to see whether the TM peptides of other proteins that are known to be targeted to lipid rafts and/or that are known to promote late steps in membrane fusion exert similar effects on the lipid bilayer. Future studies using peptides with altered sequences will be required to find a structural explanation for the apparent sequence specificity of the lipid ordering effect of TMX31. The conserved Cys210 contributes indirectly to the targeting of HA to lipid rafts. This residue is the first of three palmitoylated Cys residues at the C-terminus. In addition to the conserved residues in the N-terminal half of the TM domain, palmitoylation of the C-terminal cysteines is essential for the insertion of HA into the rafts. The other residues at the C-terminus of the TM domain are not directly involved in targeting HA to lipid rafts. These residues may have other functions. For example, the conserved Trp208 (as well as tryptophans at the N-terminus of the TM domains of H3 group HAs) may be important for the proper positioning of the TM helices in the lipid bilayer, since tryptophans preferentially partition into lipid bilayer interfaces (*48*).

The observed oligomerization of influenza HA TM domains and the observed increase of the lipid order around these domains may also have consequences for membrane fusion. It has been known for quite some time that the TM domain of HA is critically involved in a late step of membrane fusion, namely, the breakthrough of the hemifusion diaphragm, leading to the formation of the initial fusion pore (*14*). The fusion pore does not form from hemifusion diaphragms that are stabilized by GPI-anchored HA (*14, 15*), but is promoted from transient hemifusion intermediates which are formed in the presence of wild-type HA (*49, 50*). Neither the short intraviral tail nor the three palmitoylation sites near the C-terminus are important for membrane fusion (*17, 18*). Melikyan et al. (*49*) further showed that formation of the fusion pore from the hemifusion intermediate correlates with the requirement for positive curvature of the inner (C-terminal) leaflet of the bilayer to be fused. Curvature of the outer (N-terminal) leaflet was unimportant for this late step of HA-mediated membrane fusion. It is not directly intuitive how the TM domain could affect membrane curvature. On the contrary, we observe a higher degree of order of the membrane lipids around the TM peptide. Ordering of the lipids in the vicinity of the TM domain is expected to induce (or result from) a dehydration of the membrane surface. Higher packing orders of lipids are generally correlated with lower degrees of headgroup hydration in model systems (*51, 52*). Consistent with this idea, we also observe that incorporation of TMX31 into lipid bilayers causes a small diminution of the lipid ester carbonyl band component at 1728 cm^{-1} that is known to be associated with the more hydrated form of this chemical group in lipid bilayers (*43*). Partial dehydration of the proximal membrane surface could then reduce the hydration pressure between interacting membranes and thus facilitate fusion. Amphipathic positive curvature agents (such as chlorpromazine or dibucaine) that partition into the inner membrane leaflet could accentuate this effect or otherwise enhance the probability of fusion pore formation (*49*).

The significance of oligomer formation of the influenza HA TM peptides in SDS micelles and lipid bilayers with respect to HA's ability to form fusion pores is not so clear. At least in the peptide/SDS model system, the stoichiometry of the oligomers is not well-defined; dimers up to pentamers are observed. Despite their heat-stability, the oligomers are quite dynamic and accessible to water surrounding the lipid bilayers, as judged from their ability to exchange a large fraction of amide hydrogens on a time scale of tens of minutes to several hours (Figure 6). These results suggest that the TM domain might form channels or a least structures with some water-accessible vestibules in lipid bilayer membranes. Whether this observation is directly related to the ability of HA to form ion-permeable fusion pores (*53*) is not known. In current models of membrane fusion, lipid structures are emphasized in the center of the fusion pore, and the fusion proteins are given a more peripheral role (*49, 50*). However, the high propensity of highly conserved serine and cysteine residues throughout the sequence and in a pattern that would expose them to the same face of the α-helix is intriguing and almost certainly responsible for the high degree of water accessibility that we observe.

Our CD results indicate that the helical content of the TM peptide increases as the negative surface charge density of the host lipid bilayer is increased. This could be due to electrostatic stabilizing interactions between the flanking lysine and arginine residues and the lipid bilayer. We have observed increased molar ellipticity ratios $[\theta]_{222}/[\theta]_{210}$ for the peptide in HFIP and phospholipid bilayers, but not in lysoPC micelles. The larger ratios have been reported to be indicative of coiled coils (*34, 35*), although the rotational strengths of these transitions may also depend on other factors, such as the length of α-helical segments or the polarity of the environment (*35, 54*). The aggregation of the peptides observed in SDS micelles and the low-frequency shoulder observed in the FTIR amide I′ band are supportive of the coiled coil interpretation. How and why lysoPC prevents these interactions is not entirely clear. It is possible that lysoPC is the "best" and most dynamic solvent for this peptide: The hydrophilic residues (at the ends and within the sequence) may prefer to be most shielded from the highly apolar organic solvent and the more condensed apolar interior of the lipid bilayer. Consistent with this idea is our finding that the peptide exhibits extremely low solubilities in all organic solvents (except HFIP) that we tested and that prior solubilization in lysoPC was necessary to successfully reconstitute this peptide into lipid bilayers. LysoPC is an amphipathic positive curvature agent like the previously mentioned chlorpromazine and dibucaine that promote fusion by action of the inner leaflet of the viral membrane. Perhaps, a dispersion of the TM domain oligomer by positive curvature agents is important in a late step of membrane fusion.

The polarized ATR-FTIR results show that the helices of the TM peptide are aligned almost perpendicular to the plane of the membrane. Depending on the peptide concentration in the bilayer, we obtained "average" tilt angles from the membrane normal between 0 and 26°. These calculations were based on the "thin film" approximation, which we believe is the best of the currently available models to

describe orientations of peptides that are completely inserted into lipid bilayers. Other investigators have argued that the "two-phase" model is more adequate to determine order parameters from the measured dichroic ratios (*55*). We think that the two-phase model is more appropriate to describe orientational distributions of the soluble portions of membrane-bound molecules (see, e.g., ref *56*) and, therefore, is less likely to apply here. Nevertheless, if our experimental data had been evaluated with the two-phase model, we would have obtained average tilt angles between 28 and 37° from the bilayer normal. Therefore, 37° obtained by this model provides an upper bound for the average angle of the TM peptide in the "worst case" parameter scenario.

Our ^{13}C-edited FTIR spectra demonstrate the usefulness of this relatively new method to probe the local structure of interacting helices. For signal/noise reasons in recordings of single bilayer spectra, we did not attempt to measure peptides that were labeled at a single residue. Rather, we started with peptides that were simultaneously labeled at three or four close residues. Therefore, 10−13% of the amide I′ signal should arise from the labeled peptide bonds. Since the amide carbonyl carbons are labeled and since in an α-helix hydrogen bonds are formed from residue $n+4$ to residue n, labeling at residue n would probe the peptide bond between residues n and $n+1$ and the presence of α-helical secondary structure between residues n and $n+4$. We can crudely estimate the isotope effect of replacing ^{12}C with ^{13}C in a carbonyl group from the harmonic oscillator model. The oscillation frequency, ν_{ab}, of a spring between masses m_a and m_b is

$$\nu_{ab} = \frac{1}{2\pi}\sqrt{\frac{k}{\mu}} \tag{8}$$

where k is the spring constant and the reduced mass $\mu = m_a m_b/(m_a + m_b)$. Based on eq 8, we expect a shift from 1657 to 1620 cm^{-1} for a ^{12}C to ^{13}C isotope change. Normal mode calculations that were performed on a force field that was refined for polyalanine (*57*) place the ^{13}C-amide I A and E_1 modes at 1616 and 1620 cm^{-1}, respectively (S.-H. Lee and S. Krimm, personal communication).[5] Slightly larger values are expected for amide I modes of an isolated ^{13}C-amide in the neighborhood of ^{12}C-amides. For the c- and i-labeled peptides, we observed amide I bands at 1628−1631 cm^{-1} (depending on the degree of H/D exchange), i.e., ∼10 cm^{-1} above the frequencies that are expected from the model calculations. Despite this discrepancy, which may be caused by the finite length of the helices and the fact that the short ^{13}C segments have ^{12}C neighbors in our peptides, we are confident to assign the bands at 1628−1631 cm^{-1} to ^{13}C-labeled α-helix. Ludlam et al. (*58*) have assigned a band at 1614 cm^{-1} to ^{13}C-labeled α-helix, which, based on the above considerations, appears to be a relatively low frequency for an isolated ^{13}C═O group in an α-helix. Halverson et al. (*42*) measured FTIR spectra of ^{13}C-labeled β-sheet-forming peptides and found bands between 1604 and 1611 cm^{-1}, i.e., again at about 20−30 cm^{-1} lower frequencies than the corresponding unlabeled peptides. Since the bands at 1628−1631 cm^{-1} are quite resistant to H/D exchange, we consider it unlikely that they represent unordered structures, which we would expect to occur at ∼1610−1620 cm^{-1} (*41*).

The results of this paper suggest some new specific roles for the TM domain of HA at a late stage of membrane fusion. It is quite clear from these experiments that the TM domain exerts two (apparently opposing) effects on the viral membrane at the site of fusion. By ordering the lipids in its vicinity, the TM peptide alters the water structure at the bilayer−water interface in a way that renders the membrane surface more hydrophobic. Ordered lipids generally bind less water at the membrane surface, which locally reduces hydration repulsion between closely apposed lipid bilayers. At the same time, the TM oligomers allow water to penetrate deep into the membrane by virtue of a set of highly conserved hydrogen bond donating residues that line up on a ridge along the TM helices. While the membrane surface gets dehydrated, the membrane interior gets more hydrated. The balance of these interactions will destabilize the lipid bilayer structure, especially if the oligomers turn out to be dynamic and of variable stoichiometries in lipid bilayers as observed in SDS micelles. Agents that affect membrane curvature would obviously further modulate these interactions. As noted above for lysoPC, these agents may even change the oligomeric state of the TM domains. Our current view of the mechanism of HA-mediated membrane fusion is therefore as follows: (1) The hemagglutinins bind to sialic acid receptors on the target membrane. (2) The endosomal pH induces the spring-loaded conformational change of the B-loop to a helix that elongates the coiled coil of HA_2 (*3*, *4*). (3) The fusion peptide inserts into the lipid bilayer of the target membrane. (4) The coiled coils tilt with respect to the plane of the two juxtaposed membranes, which brings these membranes in closer contact (*56*, *59*). (5) The fusion peptide (see ref *13*) and the TM domain (this work) dehydrate the two respective membranes and thereby reduce hydration repulsion. (6) A mixed peptide−lipid stalk intermediate may form. (This intermediate is topologically equivalent to the hemifusion intermediate that is stabilized by the GPI-anchored HA.) (7) The fusion peptide and the TM domain cooperate to progress to the initial fusion pore, at which time electrical conductivity and contents mixing can be observed. The structures and interactions that take place in these last steps are not yet well established. For example, whether the fusion and TM peptides cooperate by direct physical interaction or indirectly through lipid intermediates will be an interesting question to further explore in the future. A tilting model that brings the fusion and TM peptides into close proximity at the fusion site has been first proposed for influenza hemagglutinin (*59*) and later adapted to HIV-mediated (*60*) and SNARE-mediated (*61*) membrane fusion. Therefore, the observations made here for the HA TM domain may be more general and may also apply to other fusion systems.

ACKNOWLEDGMENT

We thank Dr. V. Kalashnikov of the Biomolecular Research Facility at the University of Virginia for the competent synthesis of the peptides and Dr. S. Krimm (University of Michigan) for useful discussions regarding the assignment of ^{13}C-labeled amide I bands.

[5] A and E_1 are the axial and IR-active equatorial symmetry species of the amide I mode calculated for an infinite regular α-helix. The corresponding ^{12}C-amide I modes occur at 1658 and 1661 cm^{-1} (*57*).

REFERENCES

1. White, J. M. (1994) Fusion of influenza virus in endosomes: role of the hemagglutinin. in *Cellular Receptors for Animal Viruses* (Wimmer, E., Ed.) Chapter 15, pp 281−301, Cold Spring Harbor Laboratory Press, Cold Spring Harbor, NY.
2. Skehel, J. J., and Wiley, D. C. (1995) Influenza viruses and cell membranes. *Am. J. Respir. Crit. Care Med. 152*, 513−515.
3. Carr, C. M., and Kim, P. S. (1993) A spring-loaded mechanism for the conformational change of influenza hemagglutinin. *Cell 73*, 823−832.
4. Bullough, P. A., Hughson, F. M., Skehel, J. J., and Wiley, D. C. (1994) Structure of influenza haemagglutinin at the pH of membrane fusion. *Nature 371*, 37−43.
5. Wilson, I. A., Skehel, J. J., and Wiley, D. C. (1981) Structure of the haemagglutinin membrane glycoprotein of influenza virus at 3 Å resolution. *Nature 289*, 366−373.
6. Tsurudome, M., Glück, R., Graf, R., Falchetto, R., Schaller, U., and Brunner, J. (1992) Lipid interactions of the hemagglutinin HA_2 NH_2-terminal segment during influenza virus-induced membrane fusion. *J. Biol. Chem. 267*, 20225−20232.
7. Stegmann, T., Delfino, J. M., Richards, F. M., and Helenius, A. (1991) The HA2 subunit of influenza hemagglutinin inserts into the target membrane prior to fusion. *J. Biol. Chem. 266*, 18404−18410.
8. Durrer, P., Galli, C., Hoenke, S., Corti, C., Glück, R., Vorherr, T., and Brunner, J. (1996) H^+-induced membrane insertion of influenza virus hemagglutinin involves the HA2 amino-terminal fusion peptide but not the coiled coil region. *J. Biol. Chem. 271*, 13417−13421.
9. Lear, J. D., and DeGrado, W. F. (1987) Membrane binding and conformational properties of peptides representing the NH_2 terminus of influenza HA2. *J. Biol. Chem. 262*, 6500−6505.
10. Ishiguro, R., Kimura, N., and Takahashi, S. (1993) Orientation of fusion-active synthetic peptides in phospholipid bilayers: determination by Fourier transform infrared spectroscopy. *Biochemistry 32*, 9792−9797.
11. Lüneberg, J., Martin, I., Nüssler, F., Ruysschaert, J.-M., and Herrmann, A. (1995) Structure and topology of the influenza virus fusion peptide in lipid bilayers. *J. Biol. Chem. 270*, 27606−27614.
12. Gray, C., Tatulian, S. A., Wharton, S. A., and Tamm, L. K. (1996) Effect of the N-terminal glycine on the secondary structure, orientation, and interaction of the influenza hemagglutinin fusion peptide with lipid bilayers. *Biophys. J. 70*, 2275−2286.
13. Han, X., Steinhauer, D. A., Wharton, S. A., and Tamm, L. K. (1999) Interaction of mutant influenza virus hemagglutinin fusion peptides with lipid bilayers: probing the role of hydrophobic residue size in the central region of the fusion peptide. *Biochemistry 38*, 15052−15059.
14. Kemble, G. W., Danieli, T., and White, J. M. (1994) Lipid-anchored influenza hemagglutinin promotes hemifusion, not complete fusion. *Cell 76*, 383−391.
15. Melikyan, G. B., White, J. M., and Cohen, F. S. (1995) GPI-anchored influenza hemagglutinin induces hemifusion to both red blood cell and planar bilayer membranes. *J. Cell Biol. 131*, 679−691.
16. Nüssler, F., Clague, M. J., and Herrmann, A. (1997) Metastability of the hemifusion intermediate induced by glycosylphosphatidylinositol-anchored influenza hemagglutinin. *Biophys. J. 73*, 2280−2291.
17. Jin, H., Leser, G. P., Zhang, J., and Lamb, R. A. (1997) Influenza virus hemagglutinin and neuraminidase cytoplasmic tails control particle shape. *EMBO J. 16*, 1236−1247.
18. Melikyan, G. B., Jin, H., Lamb, R. A., and Cohen, F. S. (1997) The role of the cytoplasmic tail region of influenza virus hemagglutinin in formation and growth of fusion pores. *Virology 235*, 118−128.
19. Schroth-Diez, B., Ponimaskin, E., Reverey, H., Schmidt, M. F. G., and Herrmann, A. (1998) Fusion activity of transmembrane and cytoplasmic domain chimeras of the influenza virus glycoprotein hemagglutinin. *J. Virol. 72*, 133−141.
20. Skibbens, J. E., Roth, M. G., and Matlin, K. S. (1989) Differential extractability of influenza virus hemagglutinin during intracellular transport in polarized epithelial cells and nonpolar fibroblasts. *J. Cell Biol. 108*, 821−832.
21. Scheiffele, P., Roth, M. G., and Simons, K. (1997) Interaction of influenza virus hemagglutinin with sphingolipid-cholesterol membrane domains via its transmembrane domain. *EMBO J. 16*, 5501−5508.
22. Lin, S., Naim, H. Y., Rodriguez, A. C., and Roth, M. G. (1998) Mutations in the middle of the transmembrane domain reverse the polarity of transport of the influenza virus hemagglutinin in MDCK epithelial cells. *J. Cell Biol. 142*, 51−57.
23. Ten Kortenaar, P. B. W., Van Dijk, B. G., Peeters, J. M., Raaben, B. J., Adams, P. J. H. M., and Tesser G. I. (1986) Rapid and efficient method for the preparation of Fmoc-amino acids starting from 9-fluorenylmethanol. *Int. J. Pept. Protein Res. 27*, 398−400.
24. Porzio, M. A., and Pearson, A. M. (1977) Improved resolution of myofibrillar proteins with sodium dodecyl sulfate-polyacrylamide gel electrophoresis. *Biochim. Biophys. Acta 490*, 27−34.
25. Jones, L. R., Maddock, S. W., and Besch, H., Jr. (1980) Unmasking effect of alamethicin on the (Na^+, K^+)-ATPase, β-adrenergic receptor-coupled adenylate cyclase, and cAMP-dependent protein kinase activities of cardiac sarcolemmal vesicles. *J. Biol. Chem. 255*, 9971−9980.
26. Frey, S., and Tamm, L. K. (1991) Orientation of melittin in phospholipid bilayers. *Biophys. J. 60*, 922−930.
27. Tamm, L. K., and Tatulian, S. A. (1997) Infrared spectroscopy of proteins and peptides in lipid bilayers. *Q. Rev. Biophys. 30*, 365−429.
28. Tamm, L. K., and Tatulian, S. A. (1993) Orientation of functional and nonfunctional PTS permease signal sequences in lipid bilayers. A polarized attenuated total reflection infrared study. *Biochemistry 32*, 7720−7726.
29. Luo, P., and Baldwin, R. L. (1997) Mechanism of helix induction by trifluoroethanol: a framework for extrapolating the helix-forming properties of peptides from trifluoroethanol/water mixtures back to water. *Biochemistry 36*, 8413−8421.
30. Rohl, C. A., and Baldwin, R. L. (1997) Comparison of NH exchange and circular dichroism as techniques for measuring the parameters of the helix-coil transition in peptides. *Biochemistry 36*, 8435−8442.
31. Tatulian, S. A., Cortes, D. M., and Perozo, E. (1998) Structural dynamics of the *Streptomyces lividans* K^+ channel (SKC1): secondary structure characterization from FTIR spectroscopy. *FEBS Lett. 423*, 205−212.
32. Nobusawa, E., Aoyama, T., Kato, H., Suzuki, Y., Tateno, Y., and Nakajima, K. (1991) Comparison of complete amino acid sequences and receptor-binding properties among 13 serotypes of hemagglutinins of influenza A viruses. *Virology 182*, 475−485.
33. Kawaoka, Y., Yamnikova, S., Chambers, T. M., Lvov, D. K., and Webster, R. G. (1990) Molecular characterization of a new hemagglutinin, subtype H14, of influenza A virus. *Virology 179*, 759−767.
34. Cooper, T. M., and Woody, R. W. (1990) The effect of conformation on the CD of interacting helices: a theoretical study of tropomyosin. *Biopolymers 30*, 657−676.
35. Su, J. Y., Hodges, R. S., and Kay, C. M. (1994) Effect of chain length on the formation and stability of synthetic α-helical coiled coils. *Biochemistry 33*, 15501−15510.
36. Byler, D. M., and Susi, H. (1986) Examination of the secondary structure of proteins by deconvolved FTIR spectra. *Biopolymers 25*, 469−487.
37. Heimburg, T., Schuenemann, J., Weber, K., and Geisler, N. (1996) Specific recognition of coiled coils by infrared spectroscopy: analysis of the three structural domains of type III intermediate filament proteins. *Biochemistry 35*, 1375−1382.
38. Reisdorf, W. C., Jr., and Krimm, S. (1996) Infrared amide I′ band of the coiled coil. *Biochemistry 35*, 1383−1386.
39. Danieli, T., Pelletier, S. L., Henis, Y. I., and White, J. M. (1996) Membrane fusion mediated by the influenza virus

hemagglutinin requires the concerted action of at least three hemagglutinin trimers. *J. Cell Biol. 133*, 559−569.
40. Blumenthal, R., Sarkar, D. P., Durell, S., Howard, D. E., and Morris, S. J. (1996) Dilation of the influenza hemagglutinin fusion pore revealed by the kinetics of individual cell−cell fusion events. *J. Cell Biol. 135*, 63−71.
41. Tadesse, L., Nazarbaghi, R., and Walters, L. (1991) Isotopically enhanced infrared spectroscopy: a novel method for examining secondary structure at specific sites in conformationally heterogeneous peptides. *J. Am. Chem. Soc. 113*, 7036−7037.
42. Halverson, K. J., Sucholeiki, I., Ashburn, T. T., and Lansbury, P. T., Jr. (1991) Location of β-sheet-forming sequences in amyloid proteins by FTIR. *J. Am. Chem. Soc. 113*, 6701−6703.
43. Blume, A., Hübner, W., and Messner, G. (1988) Fourier transform infrared spectroscopy of $^{13}C{=}O$-labeled phospholipids hydrogen bonding to carbonyl groups. *Biochemistry 27*, 8239−8249.
44. Schroeder, R. J., Ahmed, S. N., Zhu, Y., London, E., and Brown, D. A. (1998) Cholesterol and sphingolipid enhance the Triton X-100 insolubility of glycosylphosphatidylinositol-anchored proteins by promoting the formation of detergent-insoluble ordered membrane domains. *J. Biol. Chem. 273*, 1150−1157.
45. Scheiffele, P., Rietveld, A., Wilk, T., and Simons, K. (1999) Influenza viruses select ordered lipid domains during budding from the plasma membrane. *J. Biol. Chem. 274*, 2038−2044.
46. Nezil, F. A., and Bloom, M. (1992) Combined influence of cholesterol and synthetic amphiphilic peptides upon bilayer thickness in model membranes. *Biophys. J. 61*, 1176−1183.
47. Tatulian, S. A., Jones, L. R., Reddy, L. G., Stokes, D. L., and Tamm, L. K. (1995) Secondary structure and orientation of phospholamban reconstituted in supported bilayers from polarized attenuated total reflection FTIR spectroscopy. *Biochemistry 34*, 4448−4456.
48. Wimley, W. C., and White, S. H. (1996) Experimentally determined hydrophobicity scale for proteins at membrane interfaces. *Nat. Struct. Biol. 3*, 842−848.
49. Melikyan, G. B., Brener, S. A., Ok, D. C., and Cohen, F. S. (1997) Inner but not outer membrane leaflets control the transition from glycosylphosphatidylinositol-anchored influenza hemagglutinin-induced hemifusion to full fusion. *J. Cell Biol. 136*, 995−1005.
50. Chernomordik, L. V., Frolov, V. A., Leikina, E., Bronk, P., and Zimmerberg, J. (1998) The pathway of membrane fusion catalyzed by influenza hemagglutinin: restriction of lipids hemifusion, and lipidic fusion pore formation. *J. Cell Biol. 140*, 1369−1382.
51. Lis, L. J., McAlister, M., Fuller, N., Rand, R. P., and Parsegian, V. A. (1982) Interactions between neutral phospholipid bilayer membranes. *Biophys. J. 37*, 657−665.
52. Evans, E. A., and Parsegian, V. A. (1986) Thermal-mechanical fluctuations enhance repulsion between bimolecular layers. *Proc. Natl. Acad. Sci. U.S.A. 83*, 7132−7136.
53. Spruce, A. E., Iwata, A., and Almers, W. (1991) The first milliseconds of the pore formed by a fusogenic viral envelope protein during membrane fusion. *Proc. Natl. Acad. Sci. U.S.A. 88*, 3623−3627.
54. Chen, Y.-H., Yang, J. T., and Chau, K. H. (1974) Determination of the helix and β form of proteins in aqueous solution by circular dichroism. *Biochemistry 13*, 3350−3359.
55. Citra, M. J., and Axelsen, P. H. (1996) Determination of molecular order in supported lipid membranes by internal reflection Fourier transform infrared spectroscopy. *Biophys. J. 71*, 1796−1805.
56. Gray, C., and Tamm, L. K. (1998) pH-induced conformational changes of membrane-bound influenza hemagglutinin and its effect on target lipid bilayers. *Protein Sci. 7*, 2359−2373.
57. Lee, S.-H., and Krimm, S. (1998) Ab initio-based vibrational analysis of α-poly(L-alanine). *Biopolymers 46*, 283−317.
58. Ludlam, C. F. C., Arkin, I. T., Liu, X.-M., Rothman, M. S., Rath, P., Aimoto, S., Smith, S. O., Engelman, D. M., and Rothschild, K. J. (1996) Fourier transform infrared spectroscopy and site-directed isotope labeling as a probe of local secondary structure in the transmembrane domain of phospholamban. *Biophys. J. 70*, 1728−1736.
59. Tatulian, S. A., Hinterdorfer, P., Baber, G., and Tamm, L. K. (1995) Influenza hemagglutinin assumes a tilted conformation during membrane fusion as determined by attenuated total reflection FTIR spectroscopy. *EMBO J. 14*, 5514−5523.
60. Weissenhorn, W., Dessen, A., Harrison, S. C., Skehel, J. J., and Wiley, D. C. (1997). Atomic structure of the ectodomain from HIV-1 gp41. *Nature 387*, 426−430.
61. Weber, T., Zemelman, B. V., McNew, J. A., Westermann, B., Gmachl, M., Parlati, F., Söllner, T. H., and Rothman, J. E. (1998). SNAREpins: minimal machinery for membrane fusion. *Cell 92*, 759−772.

BI991594P